AIP | Journal of Applied Physics

Electrical properties and band diagram of InSb-InAs nanowire type-III heterojunctions

A. Shik, C. Y. Chen, A. Pitanti, A. Tredicucci, D. Ercolani et al.

Citation: J. Appl. Phys. **113**, 104307 (2013); doi: 10.1063/1.4795123
View online: http://dx.doi.org/10.1063/1.4795123
View Table of Contents: http://jap.aip.org/resource/1/JAPIAU/v113/i10
Published by the American Institute of Physics.

JOURNAL OF APPLIED PHYSICS **113**, 104307 (2013)

Electrical properties and band diagram of InSb-InAs nanowire type-III heterojunctions

A. Shik,[1] C. Y. Chen,[1,a)] A. Pitanti,[2,3] A. Tredicucci,[2] D. Ercolani,[2] L. Sorba,[2] F. Beltram,[2] and H. E. Ruda[1]
[1]*Centre for Advanced Nanotechnology, University of Toronto, 170 College Street, Toronto, Ontario M5S 3E3, Canada*
[2]*NEST, Scuola Normale Superiore and Istituto Nanoscienze–CNR, Piazza San Silvestro 12, 56127 Pisa, Italy*
[3]*Thomas J. Watson Sr. Laboratory of Applied Physics, California Institute of Technology, Pasadena, California 91125, USA*

(Received 6 December 2012; accepted 25 February 2013; published online 12 March 2013)

The electrical properties of nanowire-based *n*-InSb-*n*-InAs heterojunctions were investigated theoretically and experimentally. Analysis of the current-voltage characteristics showed that the current through the heterojunction is caused mostly by generation-recombination processes in the InSb and at the heterointerface. Due to the partially overlapping valence band of InSb and the conduction band of InAs, the second process is fast and activationless. Theoretical analysis showed that, depending on the heterojunction parameters, the flux of non-equilibrium minority carriers may have a different direction, explaining the experimentally observed non-monotonic coordinate dependence of the electron beam induced current. © *2013 American Institute of Physics*. [http://dx.doi.org/10.1063/1.4795123]

I. INTRODUCTION

Among the great variety of semiconductor heterojunctions (HJs) studied and indeed used in device applications, there is a small group of so-called semimetallic HJs (sometimes called the type-III HJs) with an unusual band diagram and physical properties resembling those of semimetals, rather than semiconductors. These HJs are formed by a pair of semiconductors with noticeably different electron affinity χ, where the difference $\chi_1 - \chi_2$ exceeds the bandgap of the semiconductor with smaller χ. In such HJ, the conduction band of one semiconductor partially overlaps the valence band of the other semiconductor, and a dipole free-carrier layer consisting of electron and hole layers with equal, temperature-independent surface densities is formed at the interface. For a long time, this type of HJ, first investigated several decades ago,[1] was exemplified by GaSb-InAs, since other possible combinations suffer from strong lattice mismatch, and prevented the realization of sufficient quality material.

However, recent developments in epitaxial growth of nanowires (NWs) which can accommodate greater elastic strain than conventional planar structures,[2] opened up the possibility of expanding the choice of materials for growing defect-free type-III heterostructures. One example is the InSb-InAs heterostructure with a lattice mismatch 7% where high-quality HJs can be grown only in NW form. The system InSb-InAs has the smallest bandgap and highest electron mobility among III-V semiconductor compounds and is of potential interest for application in high speed field effect transistors,[3,4] infrared optoelectronic devices,[3,5,6] microwave[7] and terahertz[8] detectors, resonant tunneling diodes,[9] and thermoelectric devices.[3] This paper is devoted to an experimental and theoretical study of transport phenomena in this NW HJ, providing an opportunity to investigate its band diagram and the main mechanisms of conductivity. Some preliminary results of the material included in Sec. VI have already been presented.[10]

II. EXPERIMENTAL DETAILS

InSb-InAs heterostructure NWs were grown on InAs(111)B substrate by chemical beam epitaxy as described in detail in Ref. 11. The InAs section of NW had a diameter $\simeq 50$ nm, while the InSb segment was slightly thicker, due to the change in species solubility in the gold catalyst during growth. Measurements of InAs NWs fabricated using identical conditions,[12] showed them to have an n-type conductivity with a rough estimate for the electron concentration at the level of 3×10^{17} cm^{-3} and the InSb segment also showed *n*-type behaviour with a resistivity $0.2\,\Omega$cm, which corresponds to a carrier concentration $n_1 \simeq 10^{16}-10^{17}$ cm^{-3}.

It has been recently shown by a number of authors (see, e.g., Refs. 13–16) that NWs of narrow-gap III-V semiconductors may not have a zinc-blende crystalline structure, as bulk crystals, but a wurtzite one. The high-resolution TEM microscopy showed[11] that in our samples the InAs base grows with the wurtzite structure, whereas the top InSb segment crystallizes in the zinc blende phase, which agrees with the results of other authors.[17]

To fabricate the samples for measurements, InSb-InAs NWs were mechanically transferred from the growth substrate onto a p-Si substrate capped with 100 nm SiO_2, providing a backgate for tuning the device characteristics. Electron beam lithography system was used to locate NWs and define contact electrodes. Prior to metal deposition, NWs were passivated with $(NH_4)_2S_x$, to ensure a good ohmic contact between the semiconductor and metal. Finally, thermal evaporation was

a)michaelt.chen@mail.utoronto.ca.

used to deposit Ti(10 nm)/Au(130 nm) contacts. A SEM-image of the fabricated device is shown in Fig. 1.

Current-voltage characteristics (CVC) of the devices were measured in a closed-cycle helium cryostat with Keithley 4200 Semiconductor Characterization System. For investigation of the transport of minority carriers and measurements of their diffusion length, the technique of electron beam induced current (EBIC), characterized by the best spatial resolution among other methods, was chosen. The electron beam created by SEM525 (Philips) operating at 10 kV with the beam current ~150 pA and diameter ~20 nm, equipped with SEMICAPS 1000 image acquisition system, generated electron-hole pairs in some fixed point of a NW. For EBIC measurements, two electrodes shown in Fig. 1 were connected to a current preamplifier SR570 with the gain of 1 nA/V. The total capacitance of the measurement circuit was ~200 pF. To measure the temperature dependence of EBIC, a home-made liquid nitrogen cryostat was also incorporated into the SEM chamber.

III. EQUILIBRIUM BAND DIAGRAM OF HJ InSb-InAs

The band diagram of isotype *n-n*-HJ InSb-InAs has a specific form caused by anomalously high value of the electron affinity in InAs $\chi_2 = 4.9$ eV. Since the conduction band offset $\Delta E_c \equiv \chi_2 - \chi_1 = 0.31$ eV exceeds the band gap in InSb $E_{g1} = 0.17$ eV (at $T = 300$ K), the system represents a type-III HJ (see Fig. 2) where the conduction band of InAs partially overlaps the valence band of InSb, as discussed in the literature.[12,18] In our calculations, we measure energies from the conduction band edge in bulk InAs (that is at $x \to \infty$), except for the Fermi level in InSb ζ_1 (and the quasi-level ζ_3 introduced later in Sec. V), to be measured from the conduction band edge in this material at $x \to -\infty$. In this notation, both Fermi levels ζ_1 and ζ_2 are the constants determined exclusively by the corresponding doping levels.

Calculations of the HJ band diagram requires knowledge of the basic parameters of contacting semiconductors, such as band gaps, electron affinities, and carrier effective masses.

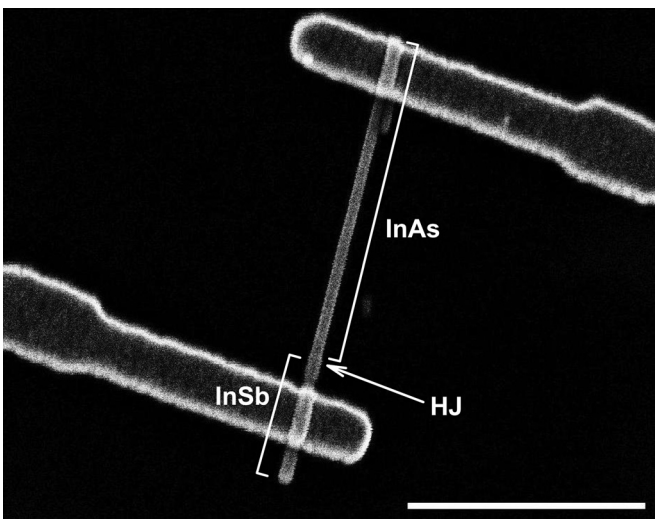

FIG. 1. SEM image of the InSb-InAs NW device. The arrow shows the HJ position and the scale bar is equal to 1 μm.

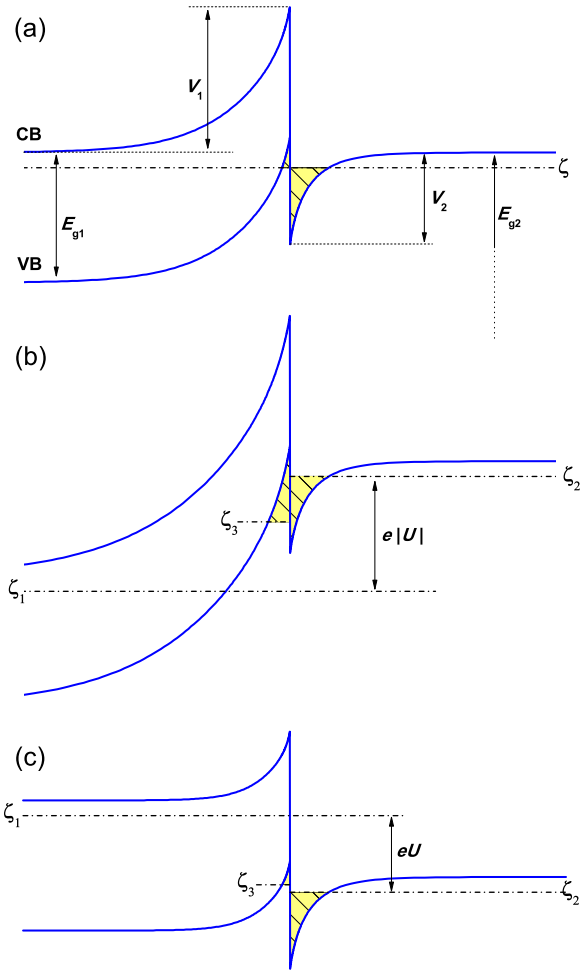

FIG. 2. Band diagram of the isotype InSb-InAs HJ in equilibrium (a), at reverse (b), and forward (c) bias. The x axis is directed along the NW with $x = 0$ at the heterointerface. The dashed areas show the accumulation layer in InAs and the inversion layer in InSb. The valence band of InAs, not participating in the carrier transport, is not shown.

Such parameters for InSb are well known but those for wurtzite InAs NWs may differ from corresponding values for bulk InAs. Unfortunately, there is few information on this account. For instance, the experimental data[16] and theoretical calculations[19] indicate that the effective mass of electrons in InAs NWs, m_{n2}, is approximately 2 times more than that in bulk InAs, so that in our future calculations we will assume $m_{n2} = 0.045m_0$. As to χ_2, then, according to Ref. 20, no reliable data are available, so that we will use the above-mentioned value of bulk InAs $\chi_2 = 4.9$ eV. It is unlikely that the real χ_2 differs from this value by more than the difference in bandgaps between the zinc-blend and wurtzite InAs, which, according to different authors,[13,19,21] lies in the interval 0.04–0.055 eV. Such variations will not undermine the inequality $\Delta E_c > E_{g1}$, resulting in the type III band diagram of Fig. 2, and hence all qualitative considerations given below.

The exact shape of the band diagram and, particularly, the band bendings V_1 and V_2 are determined by three charged layers: (1) the depletion layer of donors in InSb, (2) the electron accumulation layer in InAs, and (3) the hole inversion layer in InSb, if it exists. For calculating the profile of the accumulation layer in the InAs, we use the quasi-classical

formula for a degenerate electron gas derived in Ref. 22. Let $V(x)<0$ be the electrostatic energy profile for electrons with $V(x)=0$ at $x\to\infty$ and $V(x)=-V_1-V_2$ at $x\to-\infty$. If x_ζ is the point where the Fermi level ζ_2 crosses the conduction band edge ($V(x_\zeta)=\zeta_2$), then for $0<x<x_\zeta$ the profile $V(x)$ is determined from the equation

$$\int_{\zeta_2-V}^{\zeta_2+V_2}\frac{du}{\sqrt{\frac{32\sqrt{2}e^2m_{n2}^{3/2}}{15\pi\hbar^3\varepsilon_2}u^{5/2}+e^2E^2(x_\zeta)}}=x. \tag{1}$$

Here, ε_2 is the InAs dielectric constant and $E(x)=-\frac{1}{e}\frac{dV}{dx}$ is the local contact electric field. For the electric field at the interface, $E_2(0)$, Eq. (1) gives

$$E_2(0)=\sqrt{\frac{32\sqrt{2}m_{n2}^{3/2}}{15\pi\hbar^3\varepsilon_2}(V_2+\zeta_2)^{5/2}+E^2(x_\zeta)}. \tag{2}$$

If $\zeta_2\simeq 0$, so that $x_\zeta\to\infty$ and $E(x_\zeta)\to 0$, Eq. (1) simplifies and gives the explicit formula for $V(x)$ at $x>0$

$$V(x)=-\left[V_2^{-1/4}+x\sqrt{\frac{2\sqrt{2}e^2m_{n2}^{3/2}}{15\pi\hbar^3\varepsilon_2}}\right]^{-4}. \tag{3}$$

The doping level of the InAs $n_2\simeq 3\times10^{17}\,\mathrm{cm}^{-3}$, mentioned in Sec. II has the same order of magnitude as the effective density of states in the conduction band of InAs at room temperature, so that the assumption $\zeta_2\simeq 0$ seems quite reasonable.

Now, we consider the potential profile in InSb. In our energy scale, the edge of InSb valence band at the interface is $\Delta E_c-E_{g1}-V_2$. Then at $\zeta_2>\Delta E_c-E_{g1}-V_2$, the inversion layer in InSb is absent and the whole contact potential V_1 drops at the depletion layer creating at the interface the electric field $E_1(0)=\frac{2\sqrt{2\pi n_1V_1}}{\sqrt{\varepsilon_1}}$, where n_1 and ε_1 are the doping level and the dielectric constant in InSb, respectively. At $\zeta_2<\Delta E_c-E_{g1}-V_2$, the energy differences at the depletion and inversion layers are, respectively, $\zeta_2-\Delta E_c+E_{g1}+V_1+V_2$ and $\Delta E_c-E_{g1}-\zeta_2-V_2$. The potential profile in the inversion layer can be described by a formula similar to Eq. (1) with m_{n2} replaced by the effective mass of holes in InSb m_{p1}, corresponding changes of the integration limits, and $E(x_\zeta)$ replaced by the field of depletion layer $\frac{2\sqrt{2\pi n_1(\zeta_2-\Delta E_c+E_{g1}+V_1+V_2)}}{\sqrt{\varepsilon_1}}$. This finally gives the surface electric field in InSb $E_1(0)$, which, together with Eq. (2) and the continuity of electric induction, gives the basic equation

$$\frac{\varepsilon_2}{\varepsilon_1}\left(\frac{m_{n2}}{m_{p1}}\right)^{3/2}V_2^{5/2}=(\Delta E_c-E_{g1}-V_2-\zeta_2)^{5/2}\times\Theta(\Delta E_c-E_{g1}-V_2-\zeta_2)+\frac{15\pi^2n_1}{4\sqrt{2}m_{p1}^{3/2}}\times\min\{V_1;V_1+V_2+\zeta_2-\Delta E_c+E_{g1}\}, \tag{4}$$

TABLE I. Corresponding values of band bending for two different electron concentrations.

n_1 (cm^{-3})	V_1 (eV)	V_2 (eV)
10^{16}	0.16	0.11
10^{17}	0.21	0.12

where $\Theta(x)$ is the unit step function. Together with the condition of equilibrium

$$V_1+V_2=\Delta E_c+\zeta_1-\zeta_2, \tag{5}$$

Eq. (4) allows a determination of the values V_1, V_2 and hence the whole band diagram of the HJ.

We calculate the equilibrium HJ band diagram at the room temperature, with the parameters characterizing InSb and InAs $E_{g1}=0.17\,\mathrm{eV}$, $\Delta E_c=0.31\,\mathrm{eV}$, $m_{p1}=0.43m_0$, $m_{n2}=0.045m_0$, $\varepsilon_1=17.9$, $\varepsilon_2=14.6$ and assuming $n_2=3\times10^{17}\,\mathrm{cm}^{-3}$, for two different values of n_1 equal to 10^{16} and $10^{17}\,\mathrm{cm}^{-3}$. From Eqs. (4) and (5), we get the values of the band bendings which is shown in Table I.

It can be seen that in both cases, an inversion layer in the InSb is present. Due to the high density of states in this layer, the change in n_1 and hence in ζ_1, causes a noticeable variation of V_1, influencing the band bending in the InAs, V_2, much less.

IV. EXPERIMENTAL CURRENT-VOLTAGE CHARACTERISTICS

We performed detailed experimental investigations of the CVC of the NW with InSb-InAs HJ. In spite of isotype character of the HJ, the CVC had an asymmetric, rectifying character. Though the terms "forward" and "reverse" bias are not as straightforward as for an anisotype junction, we will, nevertheless, use them assuming by "forward" the voltage polarity corresponding to lower differential resistance of the HJ, which in our case is realized when the positive potential is applied to InAs. CVCs shown at Fig. 3(a) at large positive bias become linear, with the differential resistance $R_0\simeq 180\,\mathrm{k\Omega}$, almost independent of temperature and characterizing the resistance of the NW outside the HJ. After subtracting the voltage drop at R_0, we get the characteristic of HJ itself. To determine the potential barriers in the HJ, the main mechanisms for overcoming them, and the evolution of the band diagram with applied bias, we measured the temperature dependence of the current at each CVC point, and found the corresponding effective activation energy, as presented in Fig. 3(b).

The basic experimental dependencies of the CVC, revealed by Fig. 3(b), can be summarized as follows:

1. The CVC is strongly asymmetric, with the lower resistance (forward) branch corresponding to a positive voltage on the InAs.
2. The CVC always has an activated temperature dependence, with the activation energy being maximal at $U\simeq 0$.
3. At the negative bias, $U<-0.2\,\mathrm{V}$, the CVC saturates and has the activation energy $\simeq 0.14\,\mathrm{eV}$.

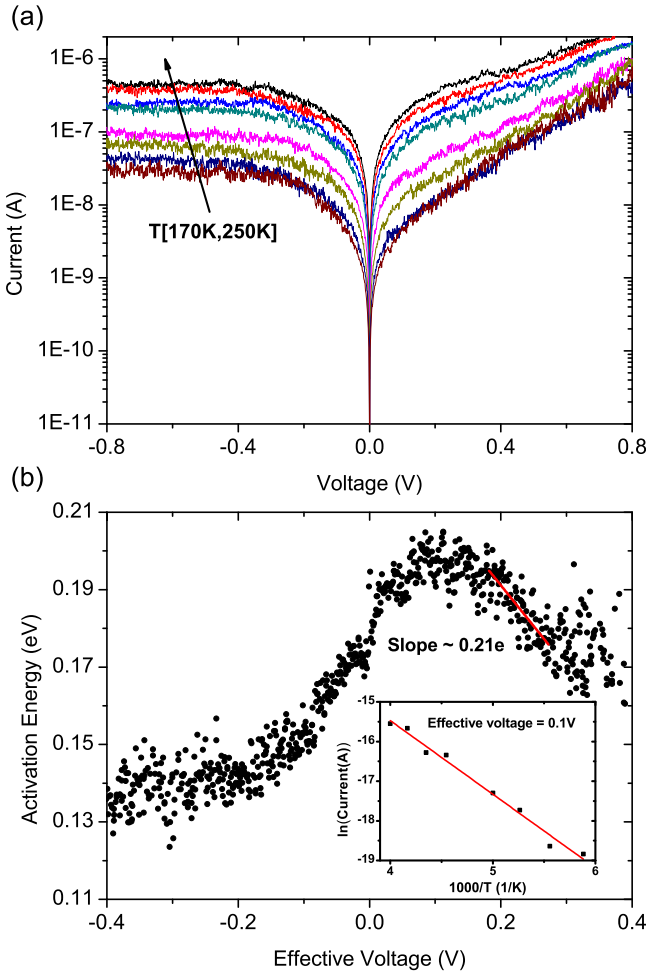

FIG. 3. CVC of the InSb-InAs HJ at different temperatures (a) and the voltage dependence of the effective activation energy of current (b). The inset in (b) gives an example of obtaining each point at the graph.

4. At the positive bias, $U > 0.1$ V, the CVC can be approximated by the expression $j \sim \exp(-\frac{\Delta_+}{kT})\exp(\frac{eU}{\eta kT})$ with the activation energy $\Delta_+ \simeq 0.2$ eV and the "non-ideality coefficient," $\eta \simeq 5$.

V. THEORETICAL CURRENT-VOLTAGE CHARACTERISTICS

The current through the HJ discussed above is now discussed as a function of the applied bias U ($U > 0$ corresponds to the positive potential applied to InAs). Since both semiconductors have n-type of conductivity, there is always the possibility of a monopolar drift-diffusion current provided by electrons overcoming the potential barrier in the conduction band equal to V_1 for the forward bias and $\Delta E_c - V_2$ for the reverse bias. However, for the band diagram of Fig. 2 containing the contact between accumulation and inversion layers at the interface, there is also an alternative current mechanism including two consecutive generation-recombination processes, one of which occurs at the heterointerface and the other, in the space charge layer, or the quasineutral region of InSb.

To estimate the relative role of these two mechanisms and find the correct expression for the whole CVC, we characterize the biased HJ by three chemical potential quasi-levels: ζ_1 and ζ_2 describing electrons, respectively, in InSb and InAs and ζ_3 describing holes in InSb, if an inversion layer exists. The first two levels are coupled by the requirement $\zeta_1 - \zeta_2 = eU$. If the current through the HJ has a monopolar character, then the generation-recombination current through the interface is negligible and quasi-levels of the inversion and accumulation layers coincide, which in our notations means $\zeta_2 = \zeta_3 + \Delta E_c - V_1 - V_2$. In this case, the band diagram of the biased HJ is described with the same equations, Eqs. (4) and (5), where in the right side of Eq. (5), the term $-eU$ should be added. As indicated in Sec. III, due to the high density of states in the accumulation layer, the band bending V_2 is practically independent of ζ_1 or, in our case, of the applied voltage U. This means that the forward branch of the CVC should have the character $\exp(eU/kT) - 1$, while the reverse one saturates and has a temperature dependence with activation energy $\simeq 0.19$ eV. Both these features contradict the experimental data described in Sec. IV, which indicates that the current through the HJ is governed, to a great extent, by the generation-recombination processes.

Thus for $U < 0$, we have the following current mechanism. The interband thermal generation creates electron-hole pairs in the InSb, which are separated by the contact electric field. Electrons go to the external contact, while holes approach the heterointerface and recombine with the electrons coming from the bulk of the InAs and providing the continuity of current in the circuit. For $U > 0$, the recombination and generation processes change places. The volume and interface generation-recombination act in series and should be characterized by the same resulting current j. This condition of current continuity determines the value of the quasi-level ζ_3.

For a more detailed analysis, we describe the volume recombination in terms of a single recombination level with binding energy E_i, concentration M, and capture coefficients γ_n, γ_p, so that the corresponding current density is given by the classical Sah-Noice-Shockley model

$$j = \gamma_n\gamma_p M N_c N_v \exp\left(-\frac{E_{g1}}{kT}\right)\left[\exp\left(\frac{\zeta_1 - \zeta_3}{kT}\right) - 1\right] \times \int \frac{dx}{\gamma_p N_v\left[\exp\left(\frac{V^*(x) - \zeta_3 - E_{g1}}{kT}\right) + \exp\left(\frac{E_i - E_{g1}}{kT}\right)\right] + \gamma_n N_c\left[\exp\left(\frac{\zeta_1 - V^*(x)}{kT}\right) + \exp\left(\frac{-E_i}{kT}\right)\right]}, \quad (6)$$

where $V^*(x) = V(x) + V_1 + V_2$ is the potential profile in InSb. In contrast to the equation for a simple *p-n*-junction, the quasi-level ζ_3 in Eq. (6) is not equal to $\zeta_1 - eU$ but should be determined self-consistently. The theoretical expression for the generation-recombination current at the type-III heterojunction derived in Ref. 22 can be written in the form

$$j = \frac{e(\Delta E_c - E_{g1})^3 m_{n2}}{8\pi\hbar^3 (E_{g1}E_{g2})^{1/2}} F(\zeta_2, \zeta_3), \tag{7}$$

where the function F vanishes at $\zeta_2 = \zeta_3$ and tends to ± 1 at large $|\zeta_2 - \zeta_3|$. For the system InSb-InAs, the prefactor before F is on the order of 10^7 A/cm^2. The expressions, Eqs. (6) and (7), determine the unknown values of ζ_3 and j (that is the CVC).

For large negative U, by analogy with the theory of *p-n*-junctions, we can neglect the first terms in square brackets in the denominator of Eq. (6) describing the concentrations of free electrons and holes, which makes the integrand independent of the unknown potential profile $V^*(x)$. The resulting expression for j contains an exponentially small activation factor and is less than the prefactor before F in Eq. (7). This means that $F(\zeta_2, \zeta_3) \ll 1$, which can only be realized at very small $\zeta_2 - \zeta_3$. This allows us to replace ζ_3 in Eq. (6) by $\zeta_2 - \Delta E_c + V_1 + V_2$, so that $\exp\left(\frac{\zeta_1 - \zeta_3}{kT}\right)$ in Eq. (6) becomes equal to $\exp\left(\frac{eU}{kT}\right)$, and can be neglected. As a result, for large reverse bias, we obtain the same result as for a homojunction in InSb: the current saturates at the value

$$j_s \propto \exp\left[-\frac{\max\{E_i; E_{g1} - E_i\}}{kT}\right] \tag{8}$$

having activation energy in the interval $\{E_{g1}/2; E_{g1}\}$ depending on the position of the recombination centers in the bandgap. The experimental value of 0.14 eV (see Sec. IV) belongs exactly to this interval.

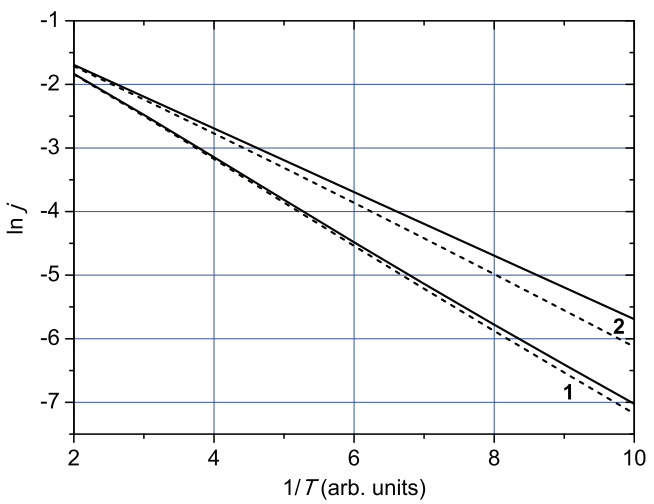

FIG. 4. Temperature dependence of the generation-recombination current at zero bias (1) and large reverse bias (2). Solid curves correspond to $E_i = 0.5E_{g1}$, dashed curves to $E_i = 0.4E_{g1}$.

For very small $|U|$, the numerator in Eq. (6) is proportional to $\zeta_1 - \zeta_3$, while in the denominator we can assume $\zeta_1 = \zeta_3$ and use for $V^*(x)$ the equilibrium expression obtained in Sec. III. The presence of the earlier ignored coordinate-dependent terms describing free carriers in the denominator of Eq. (6) changes the temperature dependence of the current, as compared to Eq. (8). To elucidate the character of this change, we perform numerical calculations on Eq. (6) assuming $\gamma_p N_v \simeq \gamma_n N_c$. The main contribution to the integral is given by those x where the Fermi level is close to the midgap, that is, in the depletion layer, which makes the exact shape of the inversion layer irrelevant and allows us to replace $V(x)$ by the quadratic Schottky potential. The results for $V_1 = 1.2E_{g1}$ (which for InSb corresponds to $V_1 = 0.21$ eV given in Table I) and two different E_i are given in Fig. 4. It is seen that the observed activation energy (the slope of the curves) for $U \simeq 0$ is larger than that for the saturation current at large negative U (Eq. (8)), in agreement with the experimental data of Fig. 3. A qualitative explanation of this change in the activation energy is most clear for $E_i = E_{g1}/2$. In this symmetric case, the activation energy for reverse bias (see Eq. (8)) is $E_{g1}/2$. At the same time, the free-carrier terms in the denominator of Eq. (6), which were ignored for reverse bias but become important at $U \simeq 0$, are different for electrons and holes, and bring asymmetry similar to the deviation of E_i from $E_{g1}/2$, and cause an increase in the effective activation energy of the current.

For positive U, the total contact potential $V_1 + V_2$ will decrease with U in accordance with the law $V_1 + V_2 = \Delta E_c - eU$ (see Eq. (5)). If V_2 remains almost independent of U and ζ_3 coincides with ζ_2, then Eq. (6) gives the standard Sah-Noice-Shockley CVC with the "non-ideality coefficient" $\eta = 2 : j \propto \exp\left(-\frac{eU}{2kT}\right)$. Larger values of η observed experimentally could be attributed to three factors missed in our calculations. First, calculations show that at positive U the inversion layer in InSb disappears, and the accumulation layer in InAs with its much lower density of states (due to $m_{n2} \ll m_{p1}$) can no longer provide pinning the Fermi level, so that the voltage drop U will be divided between V_1 and V_2. Second, the dependence of the surface generation Eq. (7) on the difference $\zeta_3 - \zeta_2$ is rather weak (sublinear, according to Ref. 22) and, to provide equality of this expression to the exponentially growing Eq. (6), ζ_3 may become to differ noticeably from ζ_2 thus making the difference $\zeta_1 - \zeta_3$ in Eq. (6) less than eU. Third, the barriers for recombining carriers, described by the coordinate-dependent terms in Eq. (6), can be partially overcome by tunneling, especially by electrons with their very small effective mass ($m_{n1} = 0.014m_0$). All these factors weaken the j vs U dependence, increasing η.

VI. MINORITY CARRIERS IN HJ InSb-InAs

We discuss non-equilibrium phenomena including the interband photocurrent and EBIC in the HJ InSb-InAs with the band diagram shown in Fig. 2. Characteristic features of these phenomena caused by generation of electron-hole pairs followed by their separation in the contact field are governed by the behavior of the minority carriers (holes).

Let us begin with the properties of non-equilibrium holes in InAs. Contrary to the case for the depletion layers, where the diffusion-drift motion of minority carriers is always directed towards the contact, such motion in the accumulation layers may have a different direction, as determined by two competing factors. On the one hand, the InSb valence band represents a potential well for the holes in the InAs and thus attracts them. On the other hand, to be captured by this well or to recombine at the interface, holes should overcome the repulsive electric field forming from the potential barrier V_2. To find the resulting distribution of the hole concentration $p(x)$ in the InAs (at $x > 0$) and the current of non-equilibrium holes, we must solve the continuity equation for holes, containing the terms describing drift in the electric field $E(x) = -\frac{1}{e}\frac{dV}{dx}$, recombination, and diffusion. For $V(x)$ given by Eq. (3), as well as for other potential profiles except for the unrealistic case $E = \text{const}(x)$, this problem cannot be solved analytically. However, accumulation layers with their high carrier concentration have a rather small width l, satisfying the condition $l \ll L_{p2}$, where $L_{p2} = \sqrt{D_{p2}\tau_{p2}}$ is the diffusion length, D_{p2} is the diffusion coefficient, and τ_{p2} is the lifetime of holes in InAs. This allows us to ignore recombination processes at $0 < x < l$ which reduces the continuity equation in this region to the requirement of current continuity: $-eD_{p2}\left[\frac{p(x)}{kT}\frac{dV}{dx} + \frac{dp(x)}{dx}\right] = j = \text{const}(x)$. The general solution of this differential equation is

$$p(x) = \left\{C - \frac{j}{eD_{p2}}\int_0^x \exp\left[\frac{V(x') - V_2}{kT}\right]dx'\right\}\exp\left[\frac{V_2 - V(x)}{kT}\right]. \tag{9}$$

From the boundary condition $p(0) = 0$ corresponding to a fast drop of the holes reaching the interface into the potential well in the InSb valence band, we get $C = 0$. By differentiating Eq. (9) and assuming $x = l$, where l is the border of space charge region ($V(l) = 0$), we obtain the relationship between p and $\frac{dp}{dx}$ at $x = l$. For $V_2 \gg kT$, the main contribution to the integral in Eq. (9) is given by small x where $V(x) \simeq V_2 - eE_2(0)x$ with $E_2(0) = -\frac{1}{e}\frac{dV}{dx}(0)$ being the electric field at the interface. This finally gives

$$p(l) = \frac{kT}{eE_2(0)}\exp\left(\frac{V_2}{kT}\right)\frac{dp}{dx}(l). \tag{10}$$

We note that our calculations and their final result Eq. (10) are valid for an arbitrary $V(x)$ and not restricted to the particular quasiclassical expression Eq. (3).

Outside the space charge region, at $x > l$, the motion of non-equilibrium holes has a purely diffusion character and $p(x) \sim \exp(\pm\frac{x}{L_{p2}})$. In our case, $l \ll L_{p2}$ we can replace l in Eq. (10) by 0 and consider this condition as the boundary condition to the diffusion equation. If the non-equilibrium holes are created by light with the uniform generation rate G, then the corresponding distribution of the hole concentration is

$$p(x) = G\tau_{p2}\left[1 - \frac{\exp\left(-\frac{x}{L_{p2}}\right)}{1 + \frac{kT}{eE_2(0)L_{p2}}\exp\left(\frac{V_2}{kT}\right)}\right]. \tag{11}$$

This expression can be used for theoretical analysis of photoelectric phenomena in our HJ.

The situation is different under conditions of EBIC when the carrier generation occurs in a narrow region determined by the diameter of electron beam, which is typically much less than L_{p2}, so that we can write the generation term in the form $G(x) = g\delta(x - x_0)$. In this case, the general solution in the region $0 < x < x_0$ is $p(x) = A\exp(\frac{x}{L_{p2}}) + B\exp(-\frac{x}{L_{p2}})$ and in the region $x > x_0$, $p(x) = C\exp(-\frac{x}{L_{p2}})$. The matching conditions at $x = x_0$ represent the continuity of $p(x)$ and the continuity of hole flux given by $A\exp(\frac{x_0}{L_{p2}}) + (C - B)\exp(-\frac{x_0}{L_{p2}}) = \frac{gL_{p2}}{D_{p2}}$. Together with the condition Eq. (10) at $x = 0$, this gives the photocurrent density in the external circuit, computed as the difference of hole fluxes right and left from the plane $x = x_0$

$$j_p = -eg\frac{\exp\left(\frac{V_2}{kT}\right) - \frac{eE_2(0)L_{p2}}{kT}}{\exp\left(\frac{V_2}{kT}\right) + \frac{eE_2(0)L_{p2}}{kT}}\exp\left(-\frac{2x_0}{L_{p2}}\right). \tag{12}$$

As in Sec. V, a positive sign of j_p corresponds to the motion of holes from right to left in Fig. 2(a). It is seen that the EBIC may have different sign depending on the relationship between the parameters V_2 and $E_2(0)$, characterizing the accumulation layer, and the diffusion length L_{p2}. For the particular model case of triangular potential $V(x)$, a similar result has been earlier obtained in Ref. 10. It differs from Eq. (12) by terms of the order $\frac{kT}{eE_2(0)L_{p2}} < \frac{V_2}{eE_2(0)L_{p2}} = \frac{l}{L_{p2}} \ll 1$.

When light or electron beam is absorbed in InSb, the resulting non-equilibrium holes move towards the interface and recombine there with electrons from InAs providing continuity of the current through the HJ, which in this case has always negative sign and is given by the same formulae as that in a Schottky diode from InSb with similar parameter and the barrier height V_1.

Fig. 5 demonstrates the results of EBIC measurements in HJs InSb-InAs (see also Ref. 10). It shows the EBIC signal as a function of the beam position along the NW and contacts to it. The signal from contact regions arises from direct absorption of the electron beam and their consequent generation of current in the external circuit, which is negative for the left electrode and positive for the right one. This current should be a fraction of the total beam current (shown by the horizontal dashed lines in the figure) proportional to the total number of absorbed electrons. This fraction, according to the figure, is several tens of percent, which is in a good agreement with the results of direct Monte-Carlo simulation[23] confirming that the contacts of our composition and thickness absorb most of the 10 kV electron beam.

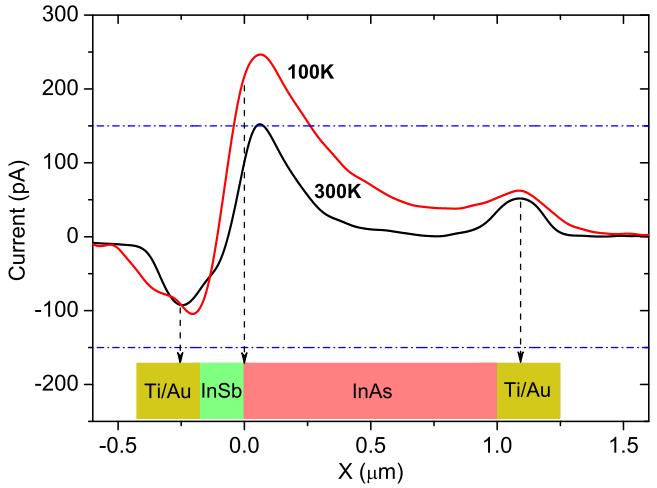

FIG. 5. Line scans of NW at 100 K (1) and 300 K (2). $x = 0$ corresponds to the InSb-InAs interface. Horizontal dashed lines show the comparison of the current in the electron beam.

When the electron beam is focused on the NW, only a minor part of the beam current is absorbed by the NW. The large EBIC signal for $-0.2\,\mu\text{m} < x < 0.9\,\mu\text{m}$, in some regions exceeding the beam current, is explained only by the multiple electron-hole pair generation by high energy electrons, which is typically characterized by the quantum yield 10^2–10^3 per primary electron.[24] The most remarkable EBIC feature, seen directly in Fig. 5, is the change of signal sign in the vicinity of the HJ, in contrast to EBIC in homo- and most HJs, where the properties of EBIC are described by the simple theory of a photodiode (see, e.g., Ref. 25). The latter predicts that the current has always the same sign, corresponding to the reverse current of the junction, and its dependence on the beam position is a single-maximum curve with the width equal to the sum of the minority carrier diffusion lengths in *n*- and *p*-regions.

The theory presented above allows us to explain the observed EBIC profile. According to Eq. (12), the sign of EBIC depends on the combination $\exp\left(\frac{V_2}{kT}\right) - \frac{eE_2(0)L_{p2}}{kT}$. For $V_2 \simeq 0.12\,\text{eV}$ (see Table I), Eq. (2) gives $E_2(0) \simeq 150\,\text{kV/cm}$ and the given combination becomes negative (and hence j_p positive) at $L_{p2} > 100\,\text{nm}$. The real value of L_{p2} in the experimental samples can be determined from the dependence of j_p on the position of electron beam x_0. By comparing the curves in Fig. 5 in the interval (0.1–0.7) μm with Eq. (12), L_{p2} was found to vary from 300 to 500 nm,[10] which corresponds to a positive sign for the EBIC. For $x_0 < 0$, that is, in the depletion layer of InSb, j_p should be negative, as in ordinary Schottky diodes, so that the observed change in the EBIC sign, is well explained.

VII. CONCLUSION

The band diagram and electrical properties of *n*-InSb- *n*-InAs NW-based narrow-gap HJs were theoretically and experimentally investigated. This pair represents a type-III (semimetallic) heterosystem, where the conduction band of InAs partially overlaps the valence band of the InSb. As a result, the HJ contains a depletion layer in the InSb, an accumulation layer in the InAs, and an inversion layer in the InSb, the latter exists at equilibrium, and at reverse bias, and disappears under forward bias. The band diagram of the HJ was calculated self-consistently, using a quasi-classical description of the accumulation and inversion layers, developed earlier by one of the authors in Ref. 22.

The CVC of the HJ was measured experimentally for a wide range of temperatures, which enabled a determination of the potential barriers overcome by carriers in for carrier transport. Analysis showed that the main current control mechanisms includes a series of two generation-recombination processes, one of which occurs in the space charge region of the InSb and is described by the classic Sah-Noice-Shockley theory, while the other has an activationless character and occurs directly at the heterointerface. In the framework of this model, all of the key characteristics of the CVC have found were well explained.

ACKNOWLEDGMENTS

Authors A.S., C.Y.C., and H.E.R. gratefully acknowledge support for this work from NSERC, CIPI, CSA, OCE, and NCE. A.P. acknowledges funding from European Union through Marie Curie Actions under REA Grant Agreement No. 298861 (NEMO).

[1]G. A. Sai-Halasz, R. Tsu, and L. Esaki, Appl. Phys. Lett. **30**, 651 (1977).
[2]K. L. Kavanagh, Semicond. Sci. Technol. **25**, 024006 (2010).
[3]P. Caroff, J. B. Wagner, K. A. Dick, H. A. Nilsson, M. Jeppsson, K. Deppert, L. Samuelson, L. R. Wallenberg, and L.-E. Wernersson, Small **4**, 878 (2008).
[4]H. A. Nilsson, P. Caroff, C. Thelander, E. Lind, O. Karlström, and L.-E. Wernersson, Appl. Phys. Lett. **96**, 153505 (2010).
[5]M. T. Bjork, B. J. Ohlsson, T. Sass, A. I. Persson, C. Thelander, M. H. Magnusson, K. Deppert, L. R. Wallenberg, and L. Samuelson, Appl. Phys. Lett. **80**, 1058 (2002).
[6]N. Panev, A. I. Persson, N. Skold, and L. Samuelson, Appl. Phys. Lett. **83**, 2238 (2003).
[7]C. Balocco, A. M. Song, M. Aberg, A. Forchel, T. Gpnzales, J. Mateos, I. Maximov, M. Missous, A. A. Rezazadeh, J. Saijets, L. Samuelson, D. Wallin, K. Williams, L. Worschech, and H. Q. Xu, Nano Lett. **5**, 1423 (2005).
[8]A. Pitanti, D. Coquillat, D. Ercolani, L. Sorba, F. Teppe, W. Knap, G. D. Simoni, F. Beltram, A. Tredicucci, and M. S. Vitiello, Appl. Phys. Lett. **101**, 141103 (2012).
[9]M. T. Bjork, B. J. Ohlsson, C. Thelander, A. I. Persson, K. Deppert, L. R. Wallenberg, and L. Samuelson, Appl. Phys. Lett. **81**, 4458 (2002).
[10]C. Y. Chen, A. Shik, A. Pitanti, A. Tredicucci, D. Ercolani, L. Sorba, F. Beltram, and H. E. Ruda, Appl. Phys. Lett. **101**, 063116 (2012).
[11]D. Ercolani, F. Rossi, A. Li, S. Roddaro, V. Grillo, G. Salvitati, F. Beltram, and L. Sorba, Nanotechnology **20**, 505605 (2009).
[12]A. Pitanti, D. Ercolani, L. Sorba, S. Roddaro, F. Beltram, L. Nasi, G. Salviati, and A. Tredicucci, Phys. Rev. X **1**, 011006 (2011).
[13]Z. Zanolli, M. E. Pistol, L. E. Froberg, and L. Samuelson, J. Phys.: Condens. Matter **19**, 295219 (2007).
[14]J. Johansson, K. A. Dick, P. Caroff, M. E. Messing, J. Bolinsson, K. Deppert, and L. Samuelson, J. Phys. Chem. C **114**, 3837 (2010).
[15]K. Kavanagh, J. Salfi, I. Savelyev, M. Blumin, and H. E. Ruda, Appl. Phys. Lett. **98**, 152103 (2011).
[16]M. H. H. Alouane, R. Anufriev, N. Chauvin, H. Khmissi, K. Naji, B. Ilahi, H. Maaref, G. Patriarche, M. Gendry, and C. Bru-Chevallier, Nanotechnology **22**, 405702 (2011).
[17]C. Thelander, P. Caroff, S. Pissard, and K. A. Dick, Appl. Phys. Lett. **100**, 232105 (2012).
[18]I. Vurgaftman, J. R. Meyer, and L. R. Ram-Mohan, J. Appl. Phys. **89**, 5815 (2001).

[19]A. De and C. E. Pryor, Phys. Rev. B **81**, 155210 (2010).
[20]S. Roddaro, K. Nilsson, G. Astromskas, L. Samuelson, L.-E. Wernersson, O. Karlstrom, and A. Wacker, Appl. Phys. Lett. **92**, 253509 (2008).
[21]M. Murayama and T. Nakayama, Phys. Rev. B **49**, 4710 (1994).
[22]A. Shik and M. Singh, Phys. Status Solidi A **168**, 195 (1998).
[23]H. Demers, N. Poirier-Demers, A. R. Couture, D. Joly, M. Guilmain, N. de Jonge, and D. Drouin, Scanning **33**, 135 (2011).
[24]H. J. Leamy, J. Appl. Phys. **53**, R51 (1982).
[25]D. B. Holt and D. C. Joy, *SEM Microcharacterization of Semiconductors* (Academic, London, 1989), Chap. 6, pp. 241–296.